Balanced carrier transport in organic solar cells employing embedded indium-tin-oxide nanoelectrodes

Min-Hsiang Hsu, Peichen Yu, Jen-Hsien Huang, Chia-Hua Chang, Chien-Wei Wu, Yu-Chih Cheng, and Chih-Wei Chu

---

Articles you may be interested in

Erratum: "Balanced carrier transport in organic solar cells employing embedded indium-tin-oxide nanoelectrodes" [Appl. Phys. Lett.98, 073308 (2011)]
Appl. Phys. Lett. **98**, 119904 (2011); 10.1063/1.3568898

Large-area organic solar cells with metal subelectrode on indium tin oxide anode
Appl. Phys. Lett. **96**, 173301 (2010); 10.1063/1.3419925

Embedded indium-tin-oxide nanoelectrodes for efficiency and lifetime enhancement of polymer-based solar cells
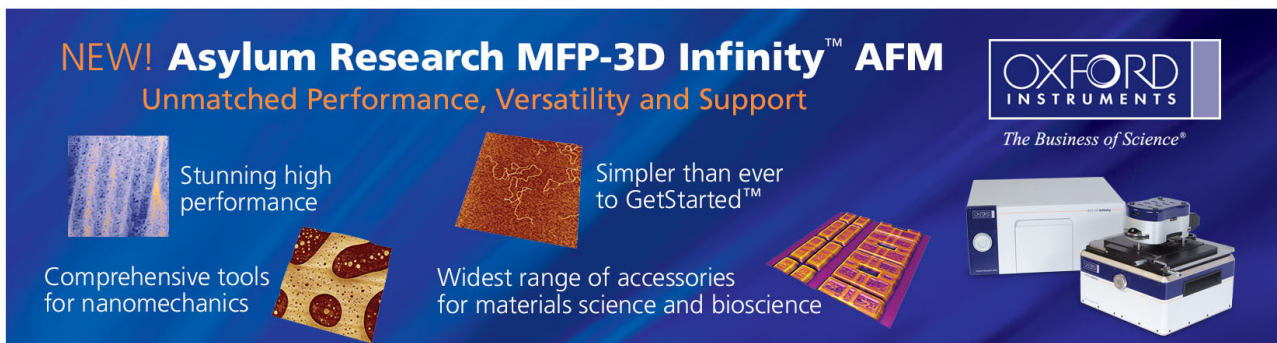Appl. Phys. Lett. **96**, 153307 (2010); 10.1063/1.3395395

Use of fluorine-doped tin oxide instead of indium tin oxide in highly efficient air-fabricated inverted polymer solar cells
Appl. Phys. Lett. **96**, 133506 (2010); 10.1063/1.3374406

Origin of the light intensity dependence of the short-circuit current of polymer/fullerene solar cells
Appl. Phys. Lett. **87**, 203502 (2005); 10.1063/1.2130396

Balanced carrier transport in organic solar cells employing embedded indium-tin-oxide nanoelectrodes

Min-Hsiang Hsu,[1,a)] Peichen Yu,[1,b)] Jen-Hsien Huang,[2,3] Chia-Hua Chang,[1] Chien-Wei Wu,[4] Yu-Chih Cheng,[1] and Chih-Wei Chu[2]

[1]*Department of Photonics and Institute of Electro-Optical Engineering, National Chiao-Tung University, Hsinchu 30010, Taiwan*
[2]*Research Center for Applied Sciences, Academia Sinica, Taipei 11529, Taiwan*
[3]*Department of Chemical Engineering, National Taiwan University, Taipei 10617, Taiwan*
[4]*Department of Electrophysics, National Chiao-Tung University, Hsinchu 30010, Taiwan*

In this paper, we present evidence of balanced electron and hole transport in polymer-fullerene based solar cells by means of embedded indium-tin-oxide nanoelectrodes. Enabled by a controllable electrochemical deposition, the individual nanoelectrodes are uniformly enclosed by a poly(3,4-ethylenedioxythiophene) hole-conducting layer, allowing a relatively short route for holes to reach the anode and hence increasing the effective hole mobility. Consequently, the power conversion efficiency and photogenerated current are maximized with a deposition condition of 50 μC, where the ratio of the electron to hole mobility is nearly unity. © *2011 American Institute of Physics*. [doi:10.1063/1.3556565]

Since solution-processed bulk-heterojunction (BHJ) solar cells were reported for organic photovoltaics (OPVs) in the mid-1990s,[1] such systems have been a popular subject of intense research. Owing to the random blends of donorlike conjugated polymers and acceptorlike fullerene molecules, strongly disordered interfaces inside the mix and hopping processes between chain segments of the conjugated polymer result in an insulatorlike behavior for organic photoactive materials.[2] Consequently, ineffective carrier conduction becomes one of the limiting factors of power conversion efficiency (PCE). Particularly, if charge transport inside the light absorbing materials is severely unbalanced, as discovered in the mixture of regioregular poly(3-hexylthiophene) (P3HT) and [6,6]-phenyl-C60-butyric acid methyl ester (PCBM), the low mobility of holes could cause charge accumulation near the anode, leading to a space charge limit current (SCLC).[3] In order to restrain the build-up space charges, major research efforts have been concentrated on adjusting the blend ratio, annealing conditions, and so on to achieve balanced carrier mobilities,[4–6] which may limit the material selection in OPVs. Although recent advances in nanofabrication technologies have permitted the formation of bicontinuous and interdigitated networks, no clear evidence has been demonstrated as to the improvement of carrier conduction.[7] In this work, we present an alternative to balance charge transport by means of buried electrodes made of indium-tin-oxide (ITO) nanorods.[8,9] The free-standing nanoelectrodes (NEs) are protruded into organic active materials, offering three-dimensional (3D) collection pathways for low mobility holes. Further enabled by a controllable electrochemical deposition (ECD) of a hole conducting layer (HCL) wrapping around individual NEs, we show evidence of balanced electron and hole transport in polymer-fullerene based solar cells.

The randomly-oriented nanorods were deposited on 260-nm-thick ITO-coated glass substrates using oblique electron-beam evaporation in an oxygen deficient environment. The rod formation involved a two-step process known as nucleation and column growth via surface diffusion, assisted by the introduced nitrogen. We have found that the obliquely incident vapor reduces the flux density of molecules on the surface, which facilitates the separation and formation of nuclei. Moreover, the oxygen deficiency allows the segregation of tin-doped indium to form a liquid surface that promotes the absorption of incident vapors, resulting in vertical column growth.[10] To function properly as embedded NEs in OPV devices, a uniform coating of a HCL enclosing the nanostructures is essential in order to effectively block electrons. Our previous work employed the conventional spin-casting of poly-(3,4-thylenedioxythiophene):poly(styrenesulfonate) (PEDOT:PSS), which exhibited poor adhesion to the NEs and slightly increased the leakage current.[10] On the other hand, the excellent conductivity of ITO NEs suggested the feasibility of a HCL via ECD.[10] The ECD process used to gradually polymerize the EDOT onto the ITO NEs is chemically scalable and controllable, and thus is relatively cost effective and also roll-to-roll compatible. Here, a triple-terminal electrochemical cell that comprised a counter, reference, and working electrode was employed with selected charge quantity settings at an applied voltage of 1.1 V. The ECD process resulted in PEDOT coatings of various thicknesses that uniformly wrapped around the 3D NEs. Figures 1(a)–1(f) show the surface morphologies of PEDOT deposited with a charge quantity setting of 0 μC, 25 μC, 50 μC, 250 μC, 500 μC on the NEs, and on a conventional 260-nm-thick ITO film at 500 μC, respectively. As shown in Fig. 1(a), the bare free-standing NEs are about 30 nm thick and 150 nm long with an estimated density of 2×10^{10} cm^{-2}. The spacing between NEs is on the order of a few tens to over a hundred nanometers, which is sufficient for the penetration of active materials without altering the organization of BHJ morphology.[11] With a charge

a)Author to whom correspondence should be addressed. Electronic mail: denilson12001@gmail.com.
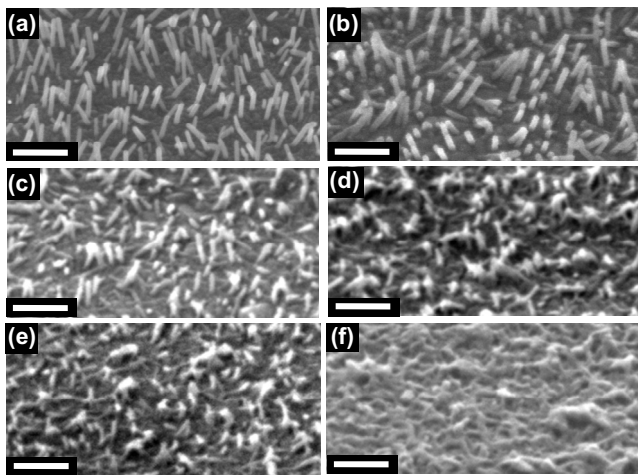b)Electronic mail: yup@faculty.nctu.edu.tw.

FIG. 1. Scanning electron microscopic images of (a) free-standing ITO nanorods deposited on a 260-nm-thick ITO film; those in (a) coated with PEDOT by ECD at (b) 25 μC, (c) 50 μC, (d) 250 μC, and (e) 500 μC. (f) The deposition of PEDOT on a controlled ITO film at 500 μC. The scalar bars are 200 nm.

FIG. 3. (Color online) The current-voltage characteristics of polymer-fullerene solar cells with embedded NEs and a controlled PE coated with PEDOT by an electrochemical method with various charge quantities: (a) short-circuit current, J_{sc}, (b) open-circuit voltage, V_{oc}, (c) FF, and (d) PCE.

setting of 25 μC, the deposited PEDOT layer is barely detectable [Fig. 1(b)]. Increasing the charge setting to 50 μC gives rise to slightly thicker NEs [Fig. 1(c)]. The deposition condition also leads to a strong electric field near the tips of NEs, resulting in a thicker PEDOT on the top than the bottom.[12] The vertical distribution of EDOT polymerization rates becomes rather discernible with large charge quantities. As seen in Figs. 1(d) and 1(e), the growth of PEDOT on the tips of NEs exceeds that on the bottom and hence forms cross-linked networks at the deposition conditions of 250 μC and 500 μC, respectively. For comparison, the deposition of PEDOT on a conventional ITO film electrode at 500 μC is shown in Fig. 1(f), which reveals a relatively dense porous structure. The coated PEDOT is ~25 nm thick.

Figures 2(a)–2(f) show the atomic force microscopic (AFM) analysis and an estimated surface roughness for structures seen in Figs. 1(a)–1(f), respectively. The morphologies of NEs shown in Fig. 2 do not resemble those in Fig. 1 which are mainly limited by the AFM tip dimension. Nevertheless, the surface analysis provides a qualitative assessment of morphology variations in ITO NEs at different deposition conditions. As seen in Figs. 2(b)–2(e), the surface
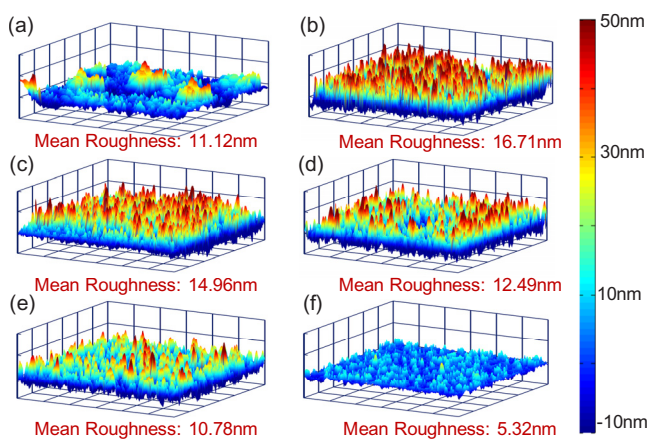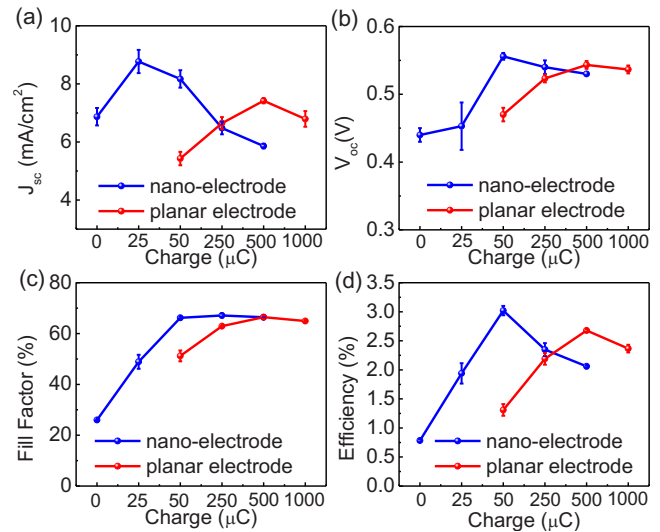

FIG. 2. (Color online) [(a)–(f)] AFM analyses for the samples shown in Figs. 1(a)–1(f), respectively.

roughness first increases at the beginning of deposition and then decreases with the increased charge settings due to a gradual planarization of the excess PEDOT. However, the surface morphology with the ITO NEs is still much rougher than that with the film electrode at the same charge quantity of 500 μC.

For practical devices, we prepared relatively short ITO NEs with heights around 100–150 nm in order to achieve adequate roughness while uniformly controlling the coating of a HCL. The 200-nm-thick active region was composed of a mixture of P3HT and PCBM with a weight ratio of 1:1 into 1,2-diochlorobenzene, which was spin-cast onto the PEDOT layer. The calcium and aluminum with respective thicknesses of 30 nm and 60 nm were subsequently capped by thermal evaporation at 10^{-5} torr. Moreover, a reference device with a conventional ITO planar electrode (PE) was fabricated with the same process procedures at the same time. The current-voltage characteristics of polymer-fullerene blended solar cells are plotted as a function of the ECD charge setting in Figs. 3(a)–3(d), which correspond to the short-circuit current density (J_{sc}), open-circuit voltage (V_{oc}), fill factor (FF), and the PCE, respectively. The cells with PEDOT on a conventional PE were first optimized with various charge settings to determine the best condition at 500 μC for reference. As seen in Fig. 3(a), the photocurrent achieves over 9 mA/cm^2 at 25 μC, and gradually deteriorates, which could result from both the planarization (Fig. 2) and parasitic absorption of PEDOT. A quick estimation based on measured transmittance spectra reveals that the absorption in PEDOT at 500 μC accounts for a decrease in J_{sc} by less than 0.3 mA/cm^2. Therefore, the planarization of PEDOT is the dominant factor in the photocurrent reduction. By comparing the NE morphologies shown in Figs. 1(c) and 1(d), the 50 μC charge setting represents a critical PEDOT layer thickness, where photocurrent is still high and the NEs remain distinctive without forming a cross-linked PEDOT network. The fast growing PEDOT at large charge settings planarizes NEs with distributed porosities and voids which diminish the purpose of embedded electrodes and hinder the device performance (Fig. 3). Nevertheless, the large photo-
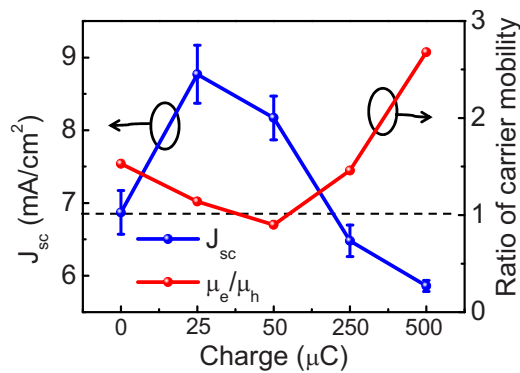
FIG. 4. (Color online) The short-circuit current J_{sc} and the ratio of electron to hole mobility (μ_e/μ_h) are plotted as a function of the charge quantity in the ECD of PEDOT.

current in Fig. 3(a) suggests that the ECD can result in a thin layer of PEDOT onto ITO nanorods with low charge settings. However, as the work function of anode also varies with the HCL thickness at the beginning of deposition,[13] an extremely thin PEDOT layer may result in a Schottky barrier on the contact, which in turn increases the saturation current and the series resistance.[14,15] Therefore, the V_{oc} and FF are relatively small at 25 μC but peaked at 50 μC, as seen in Figs. 3(b) and 3(c), respectively. Further increasing the charge setting does not affect V_{oc} and FF significantly, owing to the formation of Ohmic contacts. As a result, the cell with ITO NEs achieves the highest PCE of 3.02% with a charge quantity of 50 μC at which the condition is much lower than the best film device at 500 μC. The discrepancy in the optimized deposition condition may arise from a thicker PEDOT deposition on the NEs than on the PE with the same charge setting (see Ref. 16) for transmittance characterization). Overall, the J_{sc} and PCE are, respectively, improved by 10.1% and 13.1%, compared to the film reference. It is also worth noting that the FF achieves 66.2%, which is superior to our previous device at 58.7% using a spin-casting method for the HCL.[10] The improvement is mostly attributed to the prominent particle-by-particle electropolymerization of EDOT onto the NEs, which prevent NEs from shunting the cathode while improving the contact resistance.

The 3D NEs protruded into the photoactive material provide shorter routes for hole conduction than the PE. As a result, the time it took for holes to arrive at the anode is reduced, prompting an increase in effective hole mobility with respect to the film electrode. Under the assumption, the hole and electron mobilities can be obtained from the current-voltage characteristics of unipolar devices based on a SCLC model.[17] First, the calcium top-contact was replaced by MoO_3 by thermal evaporation to make hole-only devices. Next, Cs_2CO_3 dissolved in 2-ethoxyethanol was spin-cast

onto the ITO NEs to replace PEDOT for electron-only devices. As seen in Fig. 4, the short-circuit current density is indeed highly correlated with the ratio of the electron to hole mobility. The highest two photocurrent occurring at either 25 or 50 μC are both very close to the conditions where the mobility ratio is nearly unity. When deviating from the ideal charge settings, the electron and hole mobilities are unbalanced again, leading to a potential SCLC dictated by the quarter power of the lower carrier mobility.[3] However, as seen in Fig. 3(c), the FF at 250 and 500 μC are nearly the same, which eliminates the occurrence of a shunt current due to the SCLC. The photocurrent in these devices is most likely limited by the planarization and parasitic optical absorption of PEDOT.

[1] J. J. M. Halls, C. A. Walsh, N. C. Greenham, E. A. Marseglia, R. H. Friend, S. C. Moratti, and A. B. Holmes, Nature (London) **376**, 498 (1995).

[2] R. J. Kline, M. D. McGehee, and M. F. Toney, Nature Mater. **5**, 222 (2006).

[3] P. W. M. Blom, V. D. Mihailetchi, L. J. A. Koster, and D. E. Markov, Adv. Mater. **19**, 1551 (2007).

[4] Y. Kim, S. Cook, S. M. Tuladhar, S. A. Choulis, J. Nelson, J. R. Durrant, D. D. C. Bradley, M. Giles, I. McCulloch, C.-S. Ha, and M. Ree, Nature Mater. **5**, 197 (2006).

[5] F. Padinger, R. S. Rittberger, and N. S. Sariciftci, Adv. Funct. Mater. **13**, 85 (2003).

[6] W. Ma, C. Yang, X. Gong, K. Lee, and A. J. Heeger, Adv. Funct. Mater. **15**, 1617 (2005).

[7] B. C. Thompson and J. M. J. Fréchet, Angew. Chem., Int. Ed. **47**, 58 (2008).

[8] M. Niggemann, M. Glatthaar, A. Gombert, A. Hinsch, and V. Witter, Thin Solid Films **451–452**, 619 (2004).

[9] J. H. Huang, Z. Y. Ho, D. Kekuda, C. W. Chu, and K. C. Ho, J. Phys. Chem. C **112**, 19125 (2008).

[10] P. Yu, C. H. Chang, M. H. Su, M. H. Hsu, and K. H. Wei, Appl. Phys. Lett. **96**, 153307 (2010).

[11] S. S. V. Bavel, E. Sourty, G. D. With, and J. Loos, Nano Lett. **9**, 507 (2009).

[12] G. Marshall, P. Mocskos, H. L. Swinney, and J. M. Huth, Phys. Rev. E **59**, 2157 (1999).

[13] Y. Shi, S. C. Luo, W. Fang, K. Zhang, E. Mohamed Ali, F. Y. C. Boey, J. Y. Ying, J. Wang, H. H. Yu, and L. J. Li, Org. Electron. **9**, 859 (2008).

[14] Y. Kim, A. M. Ballantyne, J. Nelson, and D. D. C. Bradley, Org. Electron. **10**, 205 (2009).

[15] M. C. Arenas, N. Mendoza, H. Cortina, M. E. Nicho, and H. Hu, Sol. Energy Mater. Sol. Cells **94**, 29 (2010).

[16] See supplementary material at http://dx.doi.org/10.1063/1.3556565 for transmittance characterization.

[17] V. Shrotriya, Y. Yao, G. Li, and Y. Yang, Appl. Phys. Lett. **89**, 063505 (2006).